Am J Transl Res 2026;18(7):6325-6342
www.ajtr.org /ISSN:1943-8141/AJTR0173488

Original Article

Sustained-release oxymatrine hydrogel enhances the survival of transplanted placental mesenchymal stem cells and promotes wound healing in diabetic mice

Lu Liu[1,2*], Xiaodan Liu[1*], Ting Liu[1], Haibin Ma[1], Dongmei Chen[1], Shudan Liu[1]

[1]Key Laboratory of Ningxia Stem Cell and Regenerative Medicine, Institute of Medical Sciences, General Hospital of Ningxia Medical University, Yinchuan 750004, Ningxia Hui Autonomous Region, China; [2]Emergency Medicine Department, Yulin Hospital The First Affiliated Hospital of Xi'an Jiaotong University, Yulin 719000, Shaanxi, China. [*]Equal contributors.

Received April 21, 2026; Accepted June 12, 2026; Epub July 15, 2026; Published July 30, 2026

Abstract: Chronic diabetic wounds represent a significant clinical challenge due to impaired healing processes characterized by persistent inflammation, compromised angiogenesis, and a hostile microenvironment. Despite the therapeutic potential of mesenchymal stem cells (MSCs), their post-transplantation survival remains suboptimal in such pathological conditions. Here, we developed a sustained-release oxymatrine-loaded hyaluronic acid methacryloyl (HAMA) hydrogel to enhance placental mesenchymal stem cell (PMSC)-mediated repair in diabetic wounds. In a streptozotocin-induced diabetic mouse model with full-thickness dorsal skin defects, photo-crosslinked HAMA-OMT hydrogels were fabricated and evaluated for their effects on PMSC survival and wound healing outcomes. Comprehensive assessments included wound closure rates, histological analysis, angiogenesis, collagen remodeling, macrophage polarization, and the activation status of Nrf2/HO-1 and TLR4/NF-κB signaling pathways. The porous HAMA matrix provided structural support for PMSC adhesion and survival, while OMT incorporation improved hypoxia resistance and mitigated burst release kinetics. In diabetic wounds, the HAMA-OMT+PMSCs combination treatment significantly accelerated re-epithelialization, enhanced regeneration of hair follicles and sweat glands, promoted angiogenesis, and improved collagen organization compared to single-treatment groups. Mechanistically, OMT exerted dual regulatory effects by suppressing TLR4/NF-κB-driven inflammatory responses, promoting $CD206^{+}$M2 macrophage polarization, and activating Nrf2/HO-1-mediated antioxidant defenses, thereby protecting PMSCs from oxidative stress-induced apoptosis. Collectively, these findings demonstrate that OMT-loaded HAMA hydrogel synergizes with PMSCs to reconstruct a pro-regenerative microenvironment, offering a promising cell, material, and small-molecule combinatorial strategy for the effective treatment of chronic diabetic wounds.

Keywords: Oxymatrine, hydrogel, placental mesenchymal stem cells, diabetic wound healing, sustained-release, Nrf2/HO-1, NFκB

Introduction

Chronic wounds are injuries that do not progress through the normal, orderly stages of wound healing within a reasonable time frame. These wounds typically remain open for long periods and exhibit delayed or incomplete healing [1]. Current treatments for chronic wounds include specialized dressings, debridement, negative-pressure wound therapy, hyperbaric oxygen therapy, and cell- and tissue-based products [2]. However, chronic wounds are often associated with poor blood supply, ongoing inflammation, and the buildup of necrotic tissue, all of which create a hostile environment that hampers effective tissue repair [3].

In recent years, stem cell-based therapies have become a promising option for treating chronic wounds. Among these, mesenchymal stem cells (MSCs) have attracted significant interest due to their strong immunomodulatory, anti-inflammatory, and regenerative properties [4]. Adipose-derived MSCs can reduce excessive inflammation, promote new blood vessel growth, and support extracellular matrix remod-

https://doi.org/10.62347/WMUP8020

eling, thereby aiding wound healing [5]. Additionally, MSCs can differentiate into various cell types involved in tissue repair and secrete diverse cytokines and MSC-derived extracellular vesicles that promote cell growth and tissue regeneration [6]. Despite these promising results, the effectiveness of MSCs remains limited by the inflammatory, low-oxygen wound environment, and further improvements in their survival and function are needed.

Hyaluronic acid (HA)-based photopolymerized hydrogels are extensively studied as biomaterial scaffolds for wound repair. HA provides a supportive microenvironment for cell survival and growth, while methacryloyl modification enables rapid photocrosslinking with photoinitiators under ultraviolet or visible light. These hydrogels combine excellent biocompatibility, adjustable mechanical properties, and strong moisture retention, making them ideal for supporting cell adhesion, proliferation, and differentiation in wound-healing applications [7, 8].

Oxymatrine (OMT), a natural alkaloid derived from Sophora flavescens, exhibits diverse anti-inflammatory, antioxidant, antimicrobial, and immunomodulatory activities. Accumulating evidence indicates its therapeutic potential in psoriasis, parasitic infections, fungal dysbiosis, diabetic neuropathy, and atherosclerosis, where it modulates immune homeostasis, suppresses inflammatory signaling, and alleviates oxidative stress. These findings position OMT as a promising candidate for the treatment of inflammatory and metabolic disorders [9-11]. By reducing the release of inflammatory mediators, OMT may lessen inflammatory damage to cells involved in repair and improve the survival of transplanted mesenchymal stem cells in harsh conditions. Notably, OMT has demonstrated anti-apoptotic effects and may increase the viability of placental mesenchymal stem cells (PMSCs) under ischemic and hypoxic stress. However, the molecular mechanisms underlying OMT's protective effects on PMSCs, especially in refractory wound healing, remain largely unknown. Therefore, understanding the signaling pathways involved in OMT's enhancement of PMSC survival could lead to new strategies for effective chronic wound repair.

Materials and methods

Experimental animals and cells

PMSCs used in this study were obtained from the Key Laboratory of Stem Cell and Regenerative Medicine at the General Hospital of Ningxia Medical University. The collection and use of these cells were approved by the General Hospital of Ningxia Medical University's Ethics Committee (Approval No. 2020-289). PMSCs were cultured in a serum-free medium (UltraCULTURE Serum-Free Medium supplemented with Pall Ultroser G serum substitute and penicillin-streptomycin) at 37°C in a humidified incubator with 5% CO_2.

Eight-week-old specific pathogen-free (SPF) male ICR mice, weighing 25-28 g, were purchased from the Experimental Animal Center of Ningxia Medical University (licenses SCXK [Ning]2020-0001 and SYXK[Ning]2020-0001) and used with approval from the Institutional Animal Care and Use Committee (IACUC) of Ningxia Medical University (approval no. IACUC-NYLAC-2020-128). The animals were housed at the same center under standard conditions with free access to food and water. The housing environment was maintained with adequate ventilation, proper temperature and humidity, and a 12-hour light/dark cycle.

Animal experiment

Seventy-five ICR mice were fed a high-fat diet for 7 days. After a 2-hour fast, the mice were intraperitoneally injected with citrate-citric acid buffer containing streptozotocin (STZ, 150 mg/kg) [12]. Seven days post-injection, blood glucose levels were measured randomly using a Roche glucometer. Mice with blood glucose levels exceeding 16.67 mmol/L were considered to have successfully induced diabetes. The diabetic mice successfully treated were randomly assigned to the model group, hydrogel-only group, or low-, medium-, or high-dose oxymatrine groups, with 15 mice per group.

All mice were anesthetized with isoflurane before surgery. The dorsal hair was removed using depilatory cream applied with a cotton swab to the shaved area. The cream was wiped off with gauze and 75% ethanol, followed by iodophor disinfection and air drying. A full-thickness skin defect wound was created on the mid-dorsal region using a sterile 12 mm skin biopsy punch by applying rotational pressure. Any bleeding was controlled by gentle compression with sterile gauze. A sterile silicone ring was then placed around the wound and securely attached to the dry periwound skin to stabilize the defect.

The model group received no additional treatment after the wound was created. In the hydrogel-only group, 200 μL of HAMA hydrogel was applied to cover the wound, then cured with 405 nm UV light for 30 seconds before dressing and fixation. In the low-, medium-, and high-dose oxymatrine groups, 200 μL of HAMA hydrogel containing 0.2, 0.4, or 0.6 mM oxymatrine, respectively, was applied to the wound, cured under 405 nm UV light for 30 seconds, and then dressed and fixed, to allow monitoring for in vivo transdermal sustained-release experiments. After surgery, each mouse was housed individually in a separate cage. Animals underwent surgery under isoflurane inhalation anesthesia, and euthanasia was performed by isoflurane overdose in accordance with institutional animal care guidelines.

Preparation of HAMA hydrogel

HAMA (0.05 g) was dissolved in 9 mL of PBS by heating in a water bath with continuous shaking until fully solubilized. Next, 1 mL of lithium phenyl-2,4,6-trimethylbenzoyl phosphinate photoinitiator was added to the HAMA solution. The mixture was sterilized by filtration through a 0.22 μm sterile syringe filter to produce a 0.5% sterile HAMA solution. Then, 1, 2, or 4 μL of a 50 mg/mL oxymatrine solution was added to create HAMA solutions with final oxymatrine concentrations of 0.2, 0.4, or 0.6 mM, respectively. After thorough mixing, the solutions were exposed to 405 nm UV light for 30 seconds to induce crosslinking, forming colorless, transparent hydrogels. The cured hydrogels had an elastic modulus (G') of 79 Pa and a viscosity of 0.097 Pa·s.

Evaluation of wound healing

Wound healing was evaluated on days 3, 7, and 14 after treatment. The feeding behavior, mouse activity, and wound-healing progress were recorded. Digital photographs of the wounds were taken, and wound closure was measured using ImageJ software. The wound healing rate (%) was calculated with the following formula: Wound healing rate (%) = [(initial wound area - wound area at each time point)/initial wound area] × 100. The wound area was outlined with a dashed line and measured using ImageJ software.

Histopathological evaluation of wound tissue

Mice were anesthetized, and wound skin tissues were harvested and fixed in 4% paraformaldehyde for 48 hours. The tissues were dehydrated through an ethanol series, embedded in paraffin, and sectioned into 5-μm slices. After deparaffinization and rehydration, the sections were stained with hematoxylin, differentiated, blued, and then stained with eosin. The sections were then dehydrated, mounted with neutral resin, and visualized under a microscope.

Live/dead staining of PMSCs in OMT-loaded HAMA hydrogels

To study the effect of OMT on the survival of PMSCs in HAMA hydrogels, hydrogels containing 0.2, 0.4, or 0.6 mM OMT were prepared. P3 passage PMSCs were digested with trypsin, counted, and mixed with HAMA hydrogel at a density of 1.0×10^6 cells/mL. A total of 200 μL of the mixture was transferred into molds and photocrosslinked to produce HAMA+PMSCs hydrogels without OMT (HAMA+PMSCs), as well as OMT-loaded HAMA+PMSCs hydrogels (HAMA+PMSCs+OMT). The photocured hydrogels were cultured in PBS. On days 1, 2, 3, and 4, the hydrogels were stained with Calcein-AM/PI Live/Dead staining solution, photographed under a fluorescence microscope, and the proportion of live cells in each group was quantified. Cell survival rate (%) = live cells/(live cells + dead cells) × 100.

Live/dead staining of PMSCs in OMT-loaded HAMA hydrogels at diabetic wound sites

After establishing the diabetic skin defect model, mice were randomly assigned to five groups (n = 5 per group). In the sham group, skin injury surgery was performed without hydrogel coverage, whereas in the HAMA group, only hydrogel coverage was applied. In the HAMA+PMSCs group, 200 μL of HAMA hydrogel containing PMSCs at a concentration of 1.0×10^6 cells/mL was applied to the skin defect. In the HAMA+PMSCs+OMT groups, the wound was covered with 200 μL of HAMA hydrogel containing PMSCs and 0.4 mM OMT, respectively. After photocrosslinking, the wounds were bandaged, and the mice were housed individually. On days 1, 2, 3, and 4 postoperatively, the mice were euthanized, and hydrogel samples

were collected from the wound sites and placed into 6-well plates. Live/dead staining was performed using Calcein-AM/PI, and the samples were imaged via fluorescence microscopy. The proportion of viable cells in each group was then calculated.

THP-1 cell culture and treatment

The human monocytic leukemia cell line THP-1 was obtained from Hefei Wanke Biotechnology Co., Ltd. THP-1 cells were cultured in RPMI-1640 medium (Gibco, USA) supplemented with 15% fetal bovine serum (FBS; Gibco, USA), 1% penicillin-streptomycin (antibiotic-antimycotic; Gibco, USA), and 0.05 mM β-mercaptoethanol (cell culture grade) at 37°C in a humidified incubator with 5% CO_2. The cells were divided into five groups: control, LPS, OMT+LPS, PMSC-cultured medium (CM)+LPS, and high OMT+PMSC-CM+LPS. The control group cells were maintained under standard culture conditions without any treatment. The LPS group cells were treated with 0.1 μg/mL Lipopolysaccharide (LPS, MedChemExpress, China) for 24 hours.

Immunofluorescent detection of CD206 and CD68 expression in macrophages

THP-1 cells were seeded into 24-well plates and differentiated by culturing in Phorbol myristate acetate (PMA)-containing medium for 24 hours. The cells were then stimulated with 100 ng/mL interferon-γ and 100 ng/mL lipopolysaccharide, followed by OMT treatment. The grouping and treatment conditions matched those described in Section 2.1. After treatment, the cells were permeabilized with 0.5% Triton X-100 for 10 minutes and blocked with 5% BSA for 30 minutes. Cells were incubated overnight at 4°C with primary antibodies against CD206 and CD68, then for 2 hours with secondary antibodies. After DAPI staining for 5 minutes, PBS was added, and images were captured using an inverted fluorescence microscope.

5-ethynyl-2'-deoxyuridine (EdU) and immunofluorescence staining for cell proliferation

The experimental grouping and treatments matched those used in the Cell Counting Kit-8 (CCK-8) assay. After 24 hours of culture, the EdU working solution, prepared in the culture medium, was added to the cells, which were then incubated for 2 hours in a cell incubator. The cells were subsequently washed with PBS and fixed with 4% paraformaldehyde. Next, they were treated with a 2 mg/mL glycine solution, washed again with PBS, permeabilized with 0.5% Triton X-100 for 10 minutes, and twice blocked with 3% BSA in PBS. The Click-iT working solution was added, and the cells were incubated at room temperature in the dark for 30 minutes. After removing the Click-iT solution and washing twice with PBS, the Ki67 antibody (1:1,000) was added and incubated for 1 hour at room temperature. The cells were then washed twice with PBS, incubated with a fluorescent secondary antibody for 1 hour in the dark, washed twice with PBS again, and counterstained with Hoechst 33342 for 10 minutes in the dark. Finally, the cells were washed twice with PBS and imaged under a fluorescence microscope.

JC-1 staining for mitochondrial membrane potential

The grouping and treatments were the same as those used in the CCK-8 assay. After 24 hours of culture, the JC-1 working solution was added to cover the cell surface, and the cells were incubated for 15 minutes. The dye was removed, the cells were washed once with PBS, and DAPI was added for 15 minutes in the dark at room temperature. After removing the DAPI solution, the cells were washed twice with 100 μL PBS. Green and red fluorescence signals were detected using a multifunctional microplate reader, and the cells were observed under a fluorescence microscope.

Western blotting analysis

The grouping and treatments were consistent with those used in the flow cytometry assay for ROS detection. After 24 hours of culture, samples from each group were lysed, and nuclear and cytoplasmic proteins were extracted using RIPA lysis buffer. Protein concentration was measured with a BCA assay. Equal amounts of protein were loaded, separated by SDS-PAGE, and transferred onto membranes. The membranes were blocked with 5% skim milk for 1 hour and then washed three times with TBST. Primary antibodies against Nrf2, HO-1, and SOD (all 1:1,000), Lamin B1 (1:1,000), and β-actin (1:6,000) were incubated overnight at

4°C. After bringing the membranes to room temperature and washing three times with TBST, they were incubated with horseradish peroxidase-conjugated goat anti-mouse IgG and goat anti-rabbit IgG secondary antibodies (both 1:10,000) for 1 hour at room temperature. The membranes were then washed three times with TBST, developed with enhanced chemiluminescence, and analyzed by densitometry using ImageJ software.

Statistical analysis

Statistical analyses were conducted using SPSS 20.0 and GraphPad Prism 8.0. The Shapiro-Wilk test was used to assess normality. Data that followed a normal distribution were presented as mean ± standard deviation ($\bar{x} \pm s$). Comparisons among multiple groups were performed using one-way analysis of variance (ANOVA), followed by the least significant difference (LSD) test for pairwise comparisons. For data that were not normally distributed, the Kruskal-Wallis test was used for multiple-group comparisons, followed by Dunn's test for pairwise comparisons. A two-tailed significance level of $\alpha = 0.05$ was applied, and $P<0.05$ was considered statistically significant.

Results

HAMA-OMT hydrogel: preparation, structure, drug release kinetics, and effects on the survival of transplanted PMSCs in the wound environments

Given its excellent biocompatibility and biodegradability, HAMA (methacryloyl-modified hyaluronic acid) is a promising material for drug delivery. However, a key challenge in wound repair is the delivery method, as skin wounds create a highly dynamic and complex microenvironment, and few surgical or other techniques can effectively preserve and protect transplanted stem cells within the wound bed. To overcome this issue, HAMA was chosen as a delivery matrix for both cells and OMT.

The microstructure of the HAMA cell-laden hydrogel was examined using scanning electron microscopy (SEM) (**Figure 1A**). The 0.5%, 1%, and 1.5% HAMA hydrogels displayed a layered, porous internal structure with hollow features. During drying, water droplets trapped in the hydrogel evaporated, creating hemispherical pits on the inner surface. Cells adhered to and survived within the three-dimensional hydrogel network, and no significant cytotoxicity was observed at any tested concentration in vitro.

To evaluate the drug-release characteristics, hydrogels prepared with different HAMA concentrations were further analyzed. In vitro release assays showed that BSA release was relatively rapid in solution and that higher HAMA concentrations were associated with sustained release over 12 hours (**Figure 1C**). In vivo release kinetics were assessed by measuring the penetration of the lipophilic fluorescent probe DiD into cell membranes. The results indicated that the 1.5% HAMA hydrogel exhibited a slower release profile than the lower-concentration formulations (**Figure 1B**, **1D**). These findings suggest that the multilayered hydrogel structure slowed drug release, reduced the initial burst effect, and prolonged the release time in a HAMA concentration-dependent manner.

To explore the therapeutic potential of HAMA+OMT hydrogel in treating refractory wounds, a mouse full-thickness skin defect model was created on the animals' dorsal surface (**Figure 1E**). The 1% HAMA+OMT hydrogel was applied to the wound and cured with ultraviolet light. Among them, PMSCs transplanted into the hydrogel containing 0.4 mM OMT showed extended survival and higher cell viability (**Figure 1F**). Under in vitro hypoxic conditions for 24 hours, OMT also provided a protective effect on PMSC survival (**Figure 1E**, **1F**).

OMT combined with PMSCs promotes diabetic wound healing in mice

To assess the therapeutic effects of OMT and PMSCs on diabetic wound healing, an ischemic diabetic ulcer model was developed in mice, which were randomly assigned to five groups: the sham group, the HAMA hydrogel control group, the HAMA+OMT group, the HAMA+PMSCs group, and the HAMA+OMT+PMSCs group. OMT was added to commercial HAMA hydrogel at a final concentration of 0.4 mM, and 5 × 10^6 PMSCs were applied to each wound. Macroscopic analysis indicated that OMT alone, and especially OMT combined with PMSCs, significantly accelerated wound closure compared with the hydrogel control.

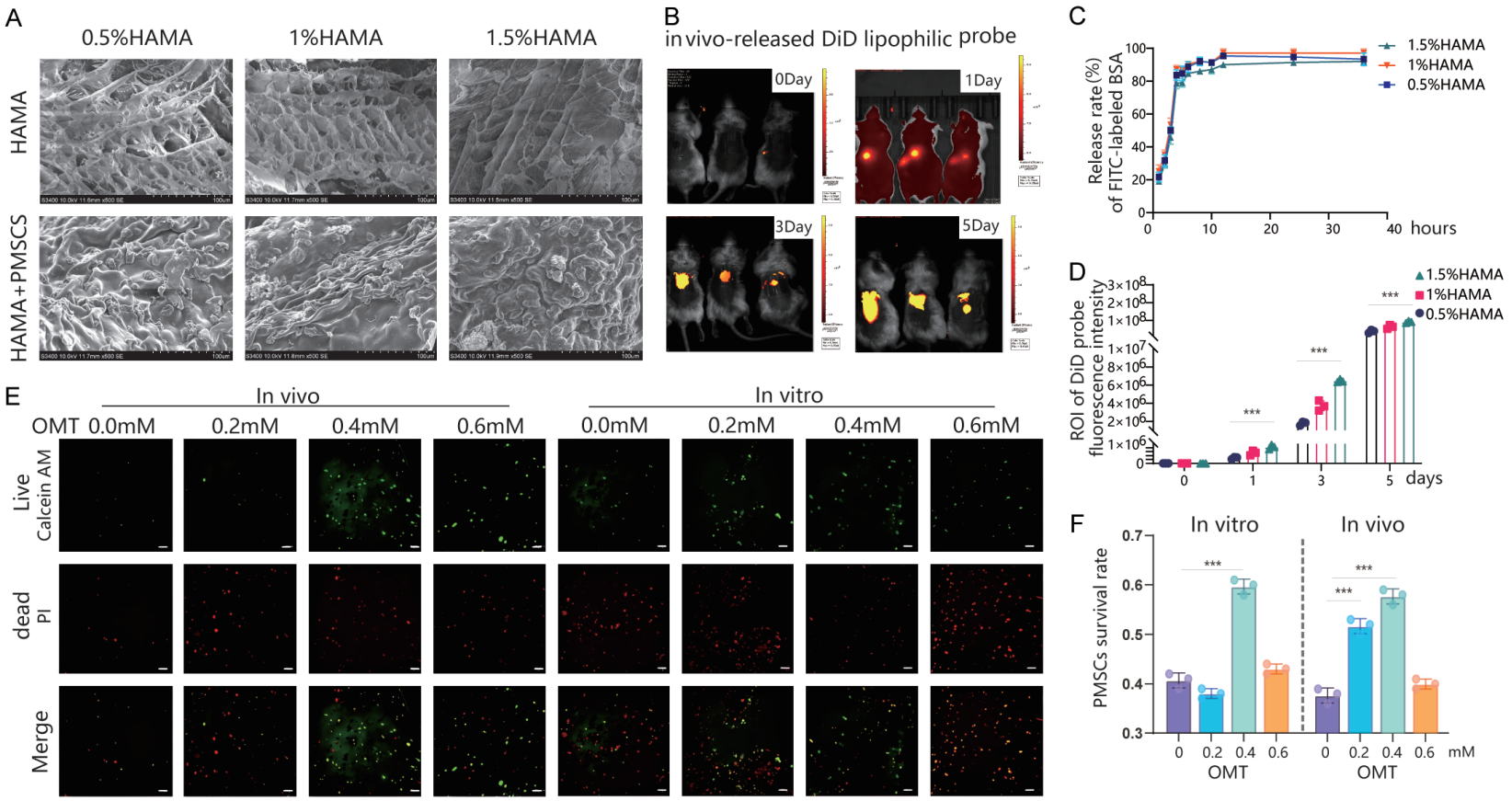

Figure 1. Characterization of hyaluronic acid methacryloyl (HAMA) hydrogels and evaluation of placental mesenchymal stem cells (PMSCs) survival and probe release behavior. A. Scanning electron microscope images of hyaluronic acid methacryloyl hydrogels with different concentrations (0.5%, 1%, 1.5%) and HAMA+PMSCs composites. Scale bars are indicated in the images and correspond to 100 μm. B. In vivo fluorescence images of DiD lipophilic probe release at 0, 1, 3, and 5 days after implantation. Color scales represent fluorescence intensity. C. Release kinetics of FITC-labeled bovine serum albumin from 0.5%, 1%, and 1.5% HAMA hydrogels over 40 hours. Data are shown as mean ± SD, n = 3. D. Quantitative analysis of DiD probe fluorescence intensity in the region of interest (ROI) at 0, 1, 3, and 5 days in vivo. $^{***}P<0.001$, n = 3. E. Live/dead staining of PMSCs cultured in HAMA hydrogels supplemented with different concentrations of oxymatrine (OMT, 0, 0.2, 0.4, and 0.6 mM) in vitro and in the wound bed. Live cells were detected in the FITC channel (Calcein AM), dead cells in the TRITC channel (PI), and merged channel images are shown. Scale bars are indicated in the images and correspond to 100 μm. F. Survival rate of PMSCs treated with various OMT concentrations under in vitro and in vivo conditions. $^{***}P<0.001$, Data are shown as mean ± SD, n = 3.

Importantly, the HAMA+PMSCs and HAMA+OMT+PMSCs groups showed quicker reduction in wound area, with significant differences on days 7 and 14. By day 7, the HAMA and HAMA+OMT groups demonstrated increased granulation tissue formation and collagen deposition, which are vital for extracellular matrix remodeling. By day 14, complete re-epithelialization was observed in the HAMA+OMT and HAMA+OMT+PMSCs groups (**Figure 2A-D**).

Hematoxylin-Eosin (H&E) staining images showed improved wound closure, increased epidermal thickness, and enhanced re-epithelialization in the HAMA+OMT+PMSCs group compared to other groups, especially on day 14. Regeneration of skin appendages, including hair follicles and sweat glands, was also more noticeable in the combined treatment group. Immunohistochemical staining indicated that the HAMA+OMT+PMSCs group had a thicker regenerated epidermis than the other groups at day 14. Additionally, the regeneration of skin appendages was more prominent in the combined treatment group (**Figure 3A**). Since wound re-epithelialization and hair follicle regeneration relies on the proliferation and differentiation of Keratin10-positive cells, their distribution was examined on day 14. Histological analysis revealed that both the HAMA+PMSCs and HAMA+OMT+PMSCs groups achieved full-thickness skin repair and re-epithelialization by day 14, with the combined group showing more significant follicular regeneration. CD31 staining demonstrated increased angiogenesis in the HAMA+PMSCs and HAMA+OMT+PMSCs groups. Masson's trichrome staining showed active collagen remodeling during wound healing, with the combined treatment group exhibiting more organized collagen deposition and a less fibrotic architecture by day 14 (**Figure 3A**). In contrast, the HAMA group displayed dense, disorganized scar-like collagen, while the OMT-only group showed limited collagen deposition. Overall, these findings suggest that both PMSCs and the combined OMT+PMSC treatment significantly improve epidermal thickness, re-epithelialization, collagen remodeling, vascular regeneration, and hair follicle regeneration, thereby accelerating diabetic wound healing. Western blot analysis confirmed that the expression levels of CD31 and col1a1 were significantly higher in the HAMA+OMT+PMSCs group compared to the control group; meanwhile, the expression of TGFβ1 was reduced in all groups except the sham group (**Figure 3B-E**).

OMT reduces M1 macrophage polarization in skin wounds by blocking TLR4

The inhibitory effect seemed to promote macrophage recruitment and differentiation in the wound microenvironment, as observed on day 7 after injury. Additionally, analysis of pro-inflammatory cytokines, including tumor necrosis factor-α, TLR4, interleukin-6 (IL-6), and p65 at the wound site, showed that, under the regulation of immunosuppressive factors secreted by mesenchymal stem cells, macrophages primarily differentiated into the M2 phenotype, while immune activation was quickly downregulated (**Figure 4A-E**). The number of CD206-labeled M2 macrophages was higher in wounds treated with OMT+PMSCs (**Figure 4F**, **4G**). Macrophages preferentially polarized toward the anti-inflammatory M2 phenotype, thereby reducing tissue damage and fibrosis caused by pro-inflammatory signaling. In vitro LPS-induced THP-1 polarization, both OMT and PMSC-conditioned medium reduced the proportion of M1 cells and increased the number of CD206-positive macrophages (**Figure 4H**, **4I**).

OMT accelerates wound healing by enhancing mitochondrial biosynthesis and activating the Nrf2/HO-1 pathway to reduce oxidative stress in local stem cells

Compared with the HAMA group, the PMSCs and OMT+PMSCs groups showed significantly increased nuclear Nrf2/Lamin B1 levels (both $P<0.05$). Total Nrf2 expression was also significantly elevated in the PMSCs and OMT+PMSCs groups versus HAMA (both $P<0.05$). For downstream antioxidant proteins, HO-1 was significantly higher in the OMT, PMSCs, and OMT+PMSCs groups compared with HAMA (all $P<0.05$), while SOD1 was markedly increased in the same three groups (OMT: $P<0.01$; PMSCs: $P<0.001$; OMT+PMSCs: $P<0.001$). Notably, the OMT+PMSCs group showed the highest overall trend in Nrf2/HO-1/SOD1-related protein expression, indicating enhanced activation of the antioxidant Nrf2/HO-1 axis in vivo (**Figure 5A-E**). Additionally, evaluation of mitochondrial damage showed that H_2O_2-treated PMSCs exhibited typical injury features, including reduced mitochondrial count, atrophy, loss of

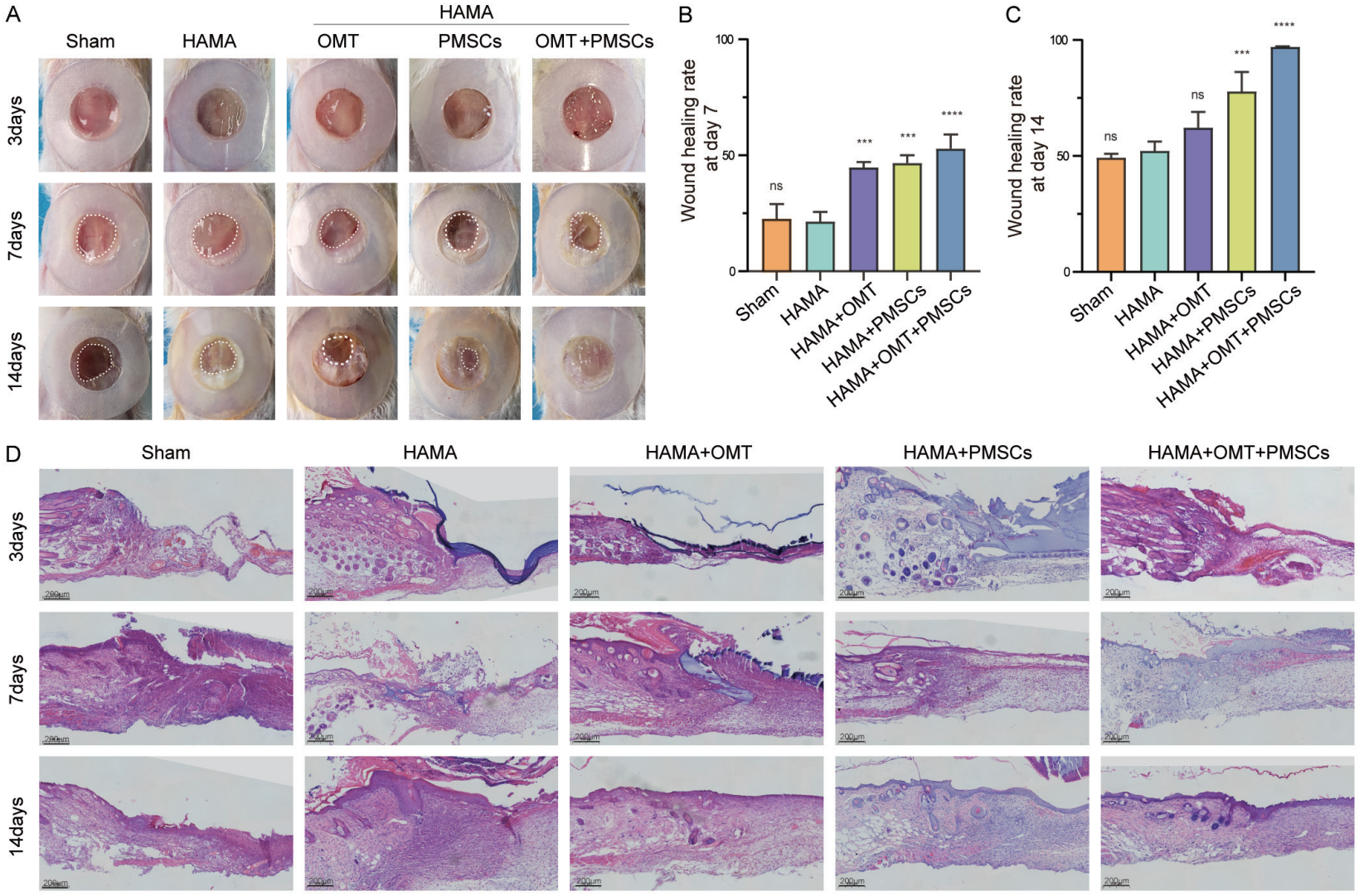

Figure 2. Oxymatrine combined with placental mesenchymal stem cells promotes diabetic wound healing in mice. A. Representative macroscopic images of wound closure across five treatment groups at 3, 7, and 14 days post-wounding. Wound boundaries are outlined with white dashed lines. B. Quantitative analysis of the wound healing rate at 7 days. C. Quantitative analysis of wound healing at 14 days. Data are shown as mean ± SD. Statistical significance: $^{***}P<0.001$, $^{****}P<0.0001$ (n = 5, sham vs. all other groups). D. Hematoxylin and eosin (H&E) staining of wound tissue sections at 3, 7, and 14 days (scale bar = 200 μm).

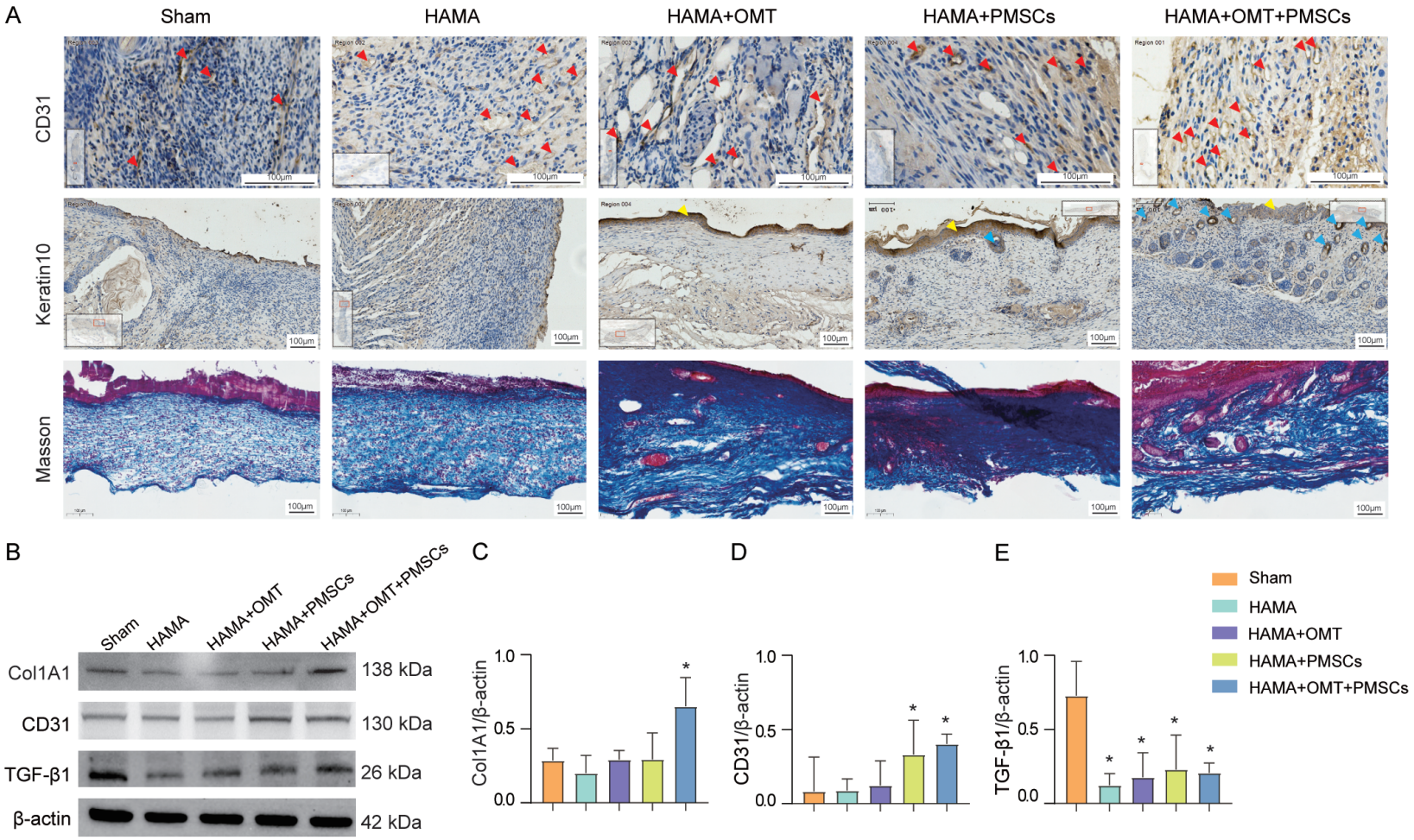

Figure 3. Oxymatrine combined with PMSCs promotes wound angiogenesis, epithelialization, and hair follicle formation. H&E staining and Masson's trichrome staining of tissue sections from different treatment groups. A. CD31 immunostaining (red arrowheads indicate CD31-positive microvessels); Keratin 10 immunostaining (yellow arrowheads: epithelial layer; blue arrowheads: hair follicle regions); Masson's trichrome staining (blue: collagen fibers; red: cytoplasm/nuclei). Scale bars: 100 μm. B. Western blot analysis of Col1A1, CD31, TGF-β1, and β-actin in tissue lysates from each group. C-E. Quantitative analysis of Western blot results. Data are presented as mean ± SD. $^{*}P<0.05$ vs sham, n = 3.

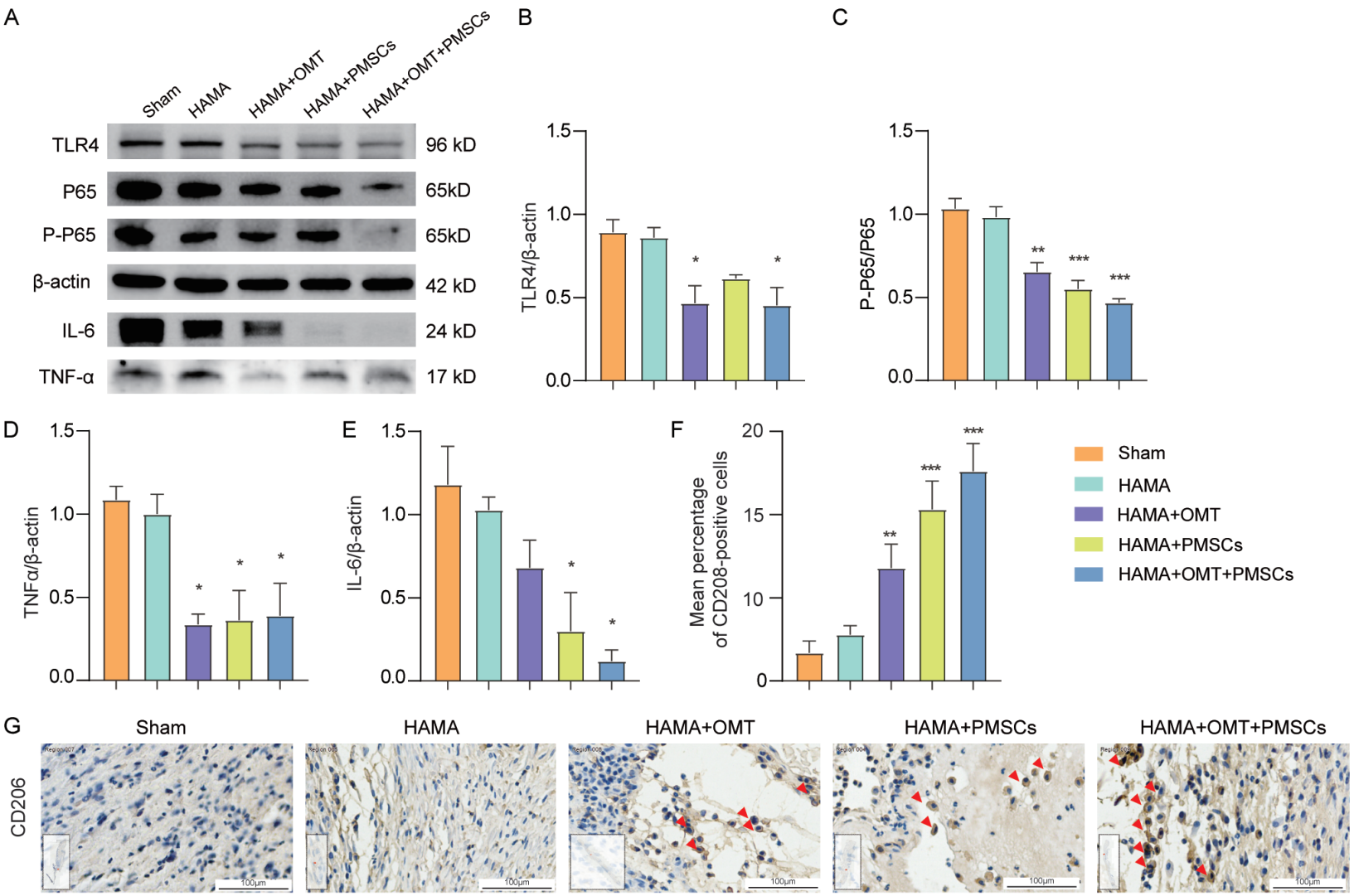
A
Sham
HAMA
HAMA+OMT
HAMA+PMSCs
HAMA+OMT+PMSCs
TLR4
P65
P-P65
β-actin
IL-6
TNF-α
96 kD
65kD
65kD
42 kD
24 kD
17 kD
B
TLR4/β-actin
C
P-P65/P65
D
TNFα/β-actin
E
IL-6/β-actin
F
Mean percentage of CD208-positive cells
Sham
HAMA
HAMA+OMT
HAMA+PMSCs
HAMA+OMT+PMSCs
G
CD206
Sham
HAMA
HAMA+OMT
HAMA+PMSCs
HAMA+OMT+PMSCs

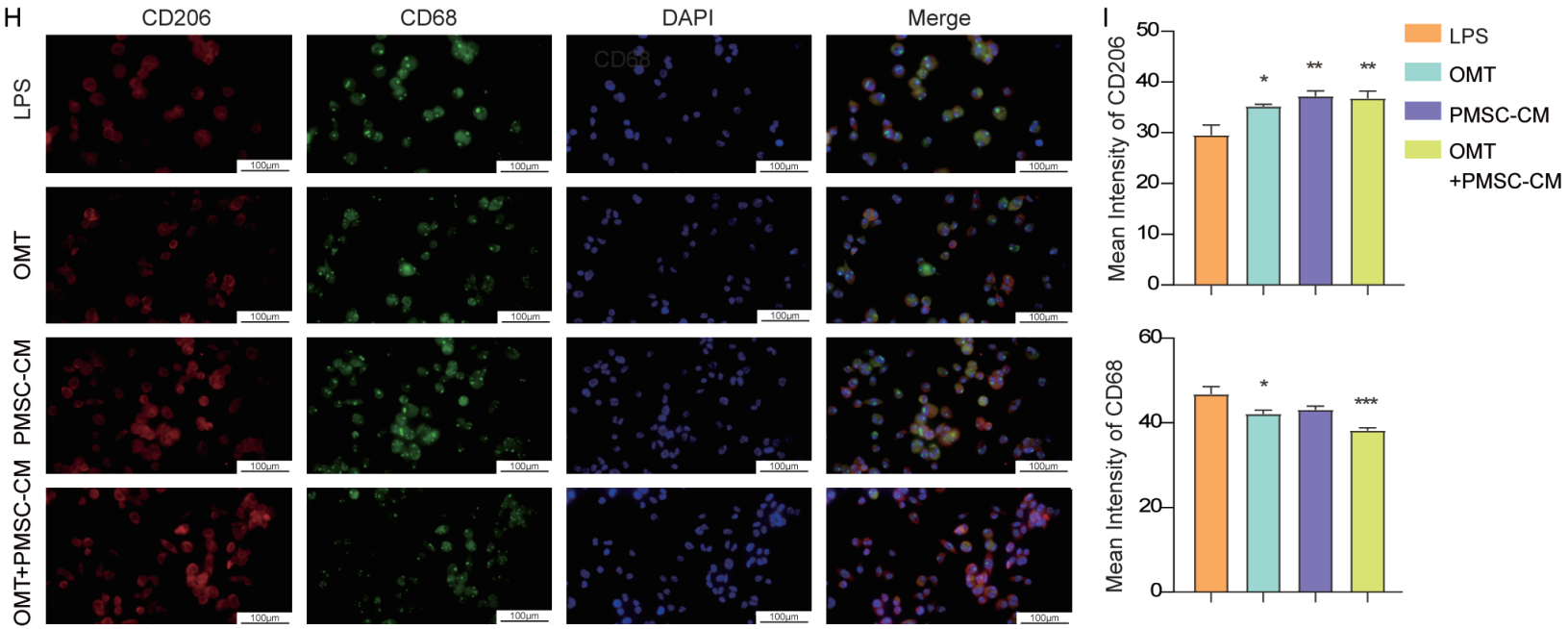

Figure 4. The effect of different treatments on the TLR4/NF-κB signaling pathway and macrophage polarization. (A) Western blot analysis of TLR4, P65, P-P65, β-actin, IL-6, and TNF-α protein expression. (B-F) Quantitative analysis of TLR4/β-actin (B), P-P65/P65 (C), TNF-α/β-actin (D), IL-6/β-actin (E), and the mean percentage of CD206-positive cells (F). (G) Immunohistochemical staining of CD206 (red arrows indicate positive cells; scale bar = 100 μm). (H) Immunofluorescence staining of CD206 (603 channel), CD68 (488nm channel), DAPI (360nm channel), and merged channel images. (scale bar = 100 μm). (I) Quantitative analysis of the mean intensity of CD206 and CD68. Data are presented as mean ± SD. $^{*}P<0.05$, $^{**}P<0.01$, $^{***}P<0.001$, n = 3.

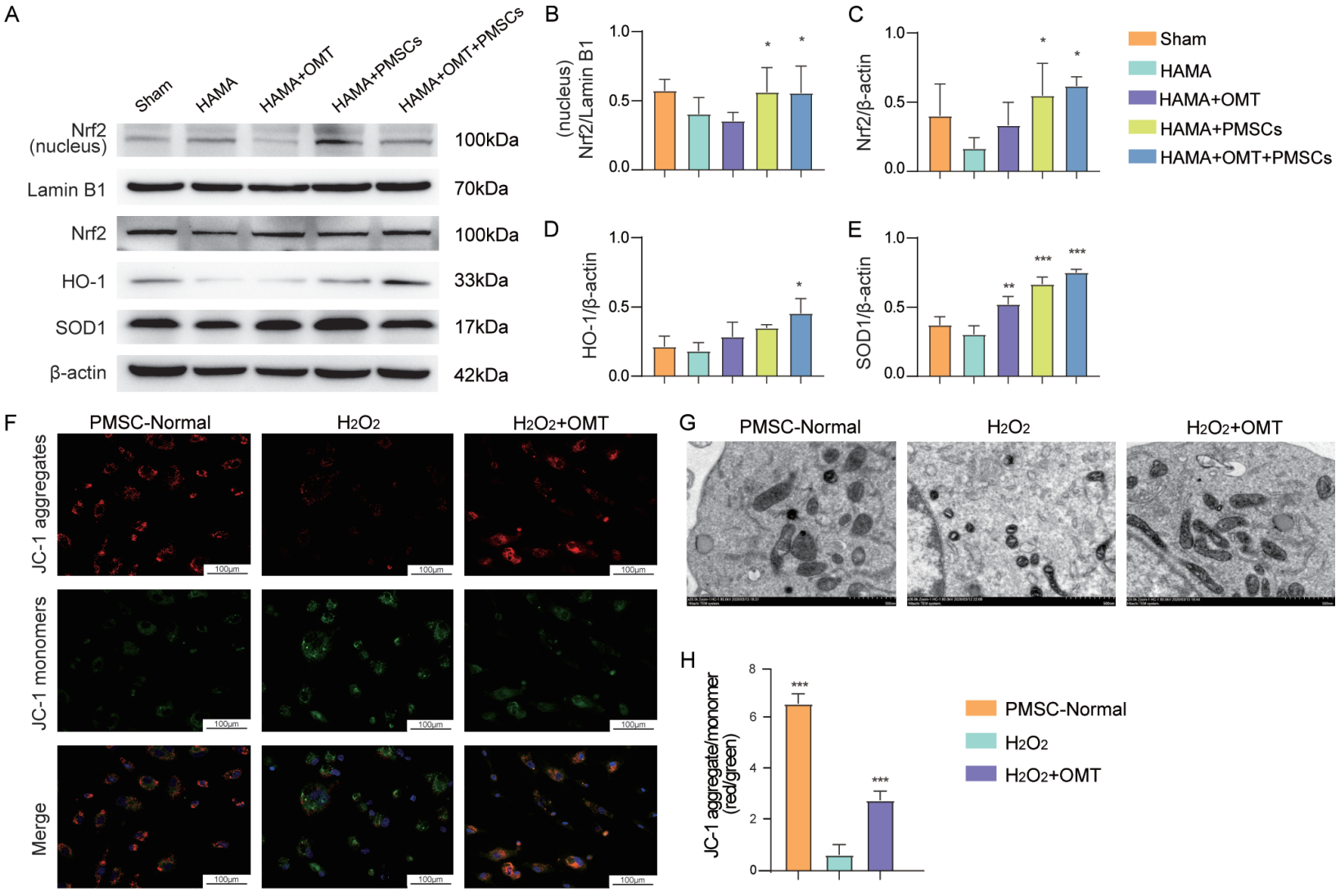
A
Sham
HAMA
HAMA+OMT
HAMA+PMSCs
HAMA+OMT+PMSCs
Nrf2 (nucleus)
Lamin B1
Nrf2
HO-1
SOD1
β-actin
100kDa
70kDa
100kDa
33kDa
17kDa
42kDa
B
(nucleus) Nrf2/Lamin B1
C
Nrf2/β-actin
Sham
HAMA
HAMA+OMT
HAMA+PMSCs
HAMA+OMT+PMSCs
D
HO-1/β-actin
E
SOD1/β-actin
F
PMSC-Normal
H2O2
H2O2+OMT
JC-1 aggregates
JC-1 monomers
Merge
100μm
G
PMSC-Normal
H2O2
H2O2+OMT
H
JC-1 aggregate/monomer (red/green)
PMSC-Normal
H2O2
H2O2+OMT

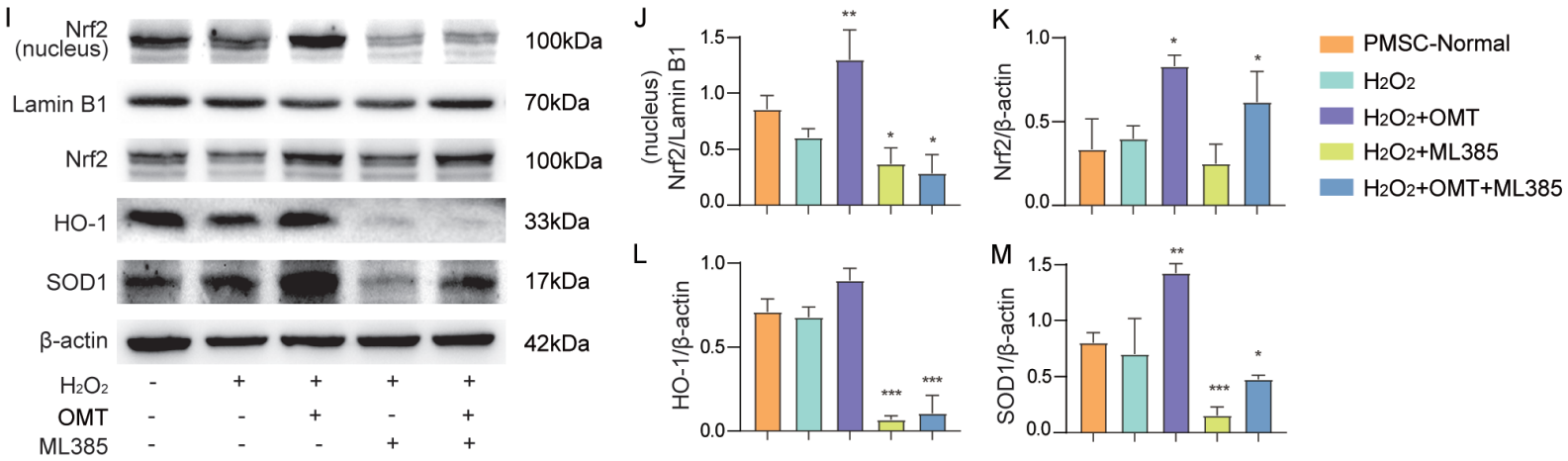

Figure 5. Oxymatrine enhancing mitochondrial biosynthesis and Nrf2/HO-1 pathway. (A) Western blot analysis of nuclear Nrf2, Lamin B1, cytoplasmic Nrf2, HO-1, SOD1, and β-actin in wound tissues from the Sham, HAMA, OMT, PMSCs, and OMT+PMSCs groups in vivo. (B-E) Quantitative analysis of nuclear Nrf2/Lamin B1 (B), cytoplasmic Nrf2/β-actin (C), HO-1/β-actin (D), and SOD1/β-actin (E) protein levels in wound tissues. (F) JC-1 staining showing mitochondrial membrane potential in PMSCs (aggregates, red; monomers, green; scale bar = 100 μm). (G) Transmission electron microscopy (TEM) images of PMSCs. (H) Quantitative analysis of the JC-1 aggregate/monomer ratio. (I-M) Quantitative analysis of nuclear Nrf2/Lamin B1 (J), cytoplasmic Nrf2/β-actin (K), HO-1/β-actin (L), and SOD1/β-actin (M) protein levels in PMSCs. Data are presented as mean ± SD. $^{*}P<0.05$, $^{**}P<0.01$, $^{***}P<0.001$, n = 3.

cristae, increased membrane density, and significant mitochondrial membrane potential depolarization (**Figure 5F**, **5G**). OMT notably restored mitochondrial morphology and structure and recovered the mitochondrial membrane potential ($P<0.001$) (**Figure 5H**).

Western blot analysis further showed that H_2O_2 stimulation reduced nuclear Nrf2 translocation and downregulated the expression of antioxidant proteins, including HO-1 and SOD1, in PMSCs (**Figure 5I-M**). In contrast, OMT treatment significantly promoted Nrf2 nuclear accumulation and increased the protein levels of HO-1 and SOD1 under oxidative stress conditions. Notably, these protective effects were largely abolished by the Nrf2 inhibitor ML385, as reflected by decreased nuclear Nrf2, HO-1, and SOD1 expression in the H_2O_2+OMT+ML385 group. Together, these findings indicate that OMT protects PMSCs against H_2O_2-induced oxidative injury, at least in part, by preserving mitochondrial function and activating the Nrf2-mediated antioxidant pathway. These results suggest that OMT reduces oxidative stress injury in PMSCs by enhancing mitochondrial function and activating the Nrf2/HO-1 pathway.

Discussion

Diabetic ulcers are characterized by persistent inflammation, excessive oxidative stress, impaired angiogenesis, and delayed tissue remodeling, all of which contribute to refractory wound healing [13, 14]. In this study, we showed that OMT combined with PMSCs transplantation significantly accelerated full-thickness wound healing and enhanced skin appendage regeneration in diabetic mice. The therapeutic effects were linked to improved keratinocyte migration, increased dermal cell activity, enhanced vascular regeneration, and modulation of the inflammatory microenvironment.

In this context, OMT has emerged as a promising therapeutic candidate due to its well-documented anti-inflammatory and antioxidant properties [15]. Accumulating evidence indicates that OMT exerts beneficial effects in a broad range of pathological conditions, including psoriasis, sepsis-induced organ injury, diabetic neuropathy, and atherosclerosis, largely through modulation of inflammatory responses and cellular stress pathways [10, 16-18]. In the present study, although the release kinetics of OMT were not directly quantified, we adopted a surrogate strategy to indirectly evaluate the diffusion behavior of the hydrogel system, as described in previous reports [19]. Specifically, fluorescently labeled BSA was used to assess macromolecular diffusion in HAMA hydrogels of different concentrations, whereas DiD was used to track lipid-associated fluorescent signals in the wound bed. Although these proxy experiments cannot substitute for direct measurement of OMT release, they nevertheless provide supportive evidence that the hydrogel possesses sustained diffusion properties.

Functionally, the combined treatment promoted keratinocyte migration and re-epithelialization, enhanced the migratory capacity of dermal fibroblasts and microvascular endothelial cells, and increased the production of repair-associated cytokines. These changes were accompanied by accelerated granulation tissue formation, improved collagen organization, and enhanced microvascular regeneration in the treated wounds. In addition, OMT combined with PMSCs appeared to facilitate extracellular matrix remodeling and wound contraction, both of which are essential for effective closure of full-thickness skin defects. Notably, the combined treatment also promoted the regeneration of skin appendages, including hair follicles. Because appendage regeneration is typically limited in refractory wounds, particularly diabetic ulcers, where persistent inflammation and impaired stromal signaling disrupt normal tissue patterning, this finding suggests that the OMT+PMSCs strategy may support a more advanced and functionally complete mode of tissue repair. Collectively, these results indicate that the combination strategy not only accelerates wound closure but also promotes more complete structural regeneration of injured skin.

A key finding of this study is that OMT significantly attenuated the inflammatory response in wound tissue. Excessive and prolonged inflammation represents a major barrier to healing in chronic wounds because it impairs the transition from the inflammatory to the proliferative phase [20]. Our data showed that OMT inhibited activation of the TLR4/NF-κB signaling pathway and reduced the expression of downstream pro-inflammatory mediators, including IL-6 and TNF-α. These changes suggest that OMT may

help restore inflammatory homeostasis. These findings suggest that OMT may restore inflammatory homeostasis and protect vascular endothelial structures from inflammatory injury [18, 21]. In addition, OMT promoted macrophage polarization toward the M2 phenotype, which is closely associated with tissue repair, extracellular matrix remodeling, and the resolution of inflammation [22, 23]. Thus, suppression of excessive inflammation together with enhancement of pro-reparative macrophage responses may represent important mechanisms underlying the beneficial effects of OMT on wound healing. Given that dysregulated inflammation and oxidative injury are central pathological features of diabetic wounds, these results further support the therapeutic potential of OMT in diabetic wound repair.

More importantly, our findings support the concept that OMT serves not merely as an anti-inflammatory agent, but as a pharmacological adjuvant that enhances PMSC-based therapy in diabetic wound healing. Rather than acting solely through an independent therapeutic effect, OMT appears to improve the wound microenvironment by alleviating oxidative stress, restraining excessive inflammation, and enhancing cell survival within the wound bed. This is particularly relevant in diabetic wounds, where the hostile pathological niche markedly compromises stem cell retention, viability, and functional efficacy after transplantation. By reshaping the local inflammatory milieu, OMT may help preserve the biological activity of PMSCs and potentiate their reparative paracrine effects, thereby amplifying the overall therapeutic efficacy of stem cell-based treatment.

This adjuvant role is consistent with previous studies showing that OMT exerts anti-inflammatory effects by modulating the TLR4/NF-κB, TLR/NF-κB, and p38 MAPK/NF-κB signaling pathways across diverse disease models [16, 24-27]. As these pathways are central mediators of inflammatory amplification and are frequently overactivated in chronic wounds, it is plausible that OMT improves the therapeutic performance of PMSCs, at least in part, by suppressing pro-inflammatory signaling and restoring a microenvironment conducive to tissue regeneration. In this context, OMT should be regarded not simply as a bioactive small molecule, but as a microenvironment-modifying adjunct that potentiates stem cell-based repair.

Mechanistically, this effect may involve coordinated regulation of inflammatory and oxidative stress pathways. NF-κB is a key regulator of chronic inflammation in diabetic wounds, where sustained activation drives the production of pro-inflammatory mediators and disrupts the normal healing process [28]. In contrast, the NRF2 pathway constitutes a major endogenous defense system against oxidative stress and is essential for maintaining redox homeostasis and supporting tissue repair [29]. Previous studies have shown that OMT can suppress NF-κB-mediated inflammatory signaling while activating NRF2-associated antioxidant responses in multiple disease models, suggesting a dual regulatory effect on inflammatory and oxidative stress pathways [18]. Therefore, it is reasonable to speculate that OMT promotes diabetic wound healing by coordinating the attenuation of inflammatory injury and the enhancement of antioxidant defense, thereby creating a more favorable environment for tissue repair.

Importantly, this combinatorial strategy may address two major barriers in diabetic wound therapy: impaired stem cell retention/function and persistent inflammatory blockade of healing. The present study, therefore, provides both mechanistic insight and translational support for incorporating OMT into PMSC-based regenerative platforms. Future studies are needed to determine whether the adjuvant effect of OMT in vivo depends predominantly on NF-κB signaling suppression, NRF2-related antioxidant program activation, or coordinated regulation of both pathways.

Similarly, OMT appears to augment PMSC function under ischemic and hypoxic conditions. The wound microenvironment is characterized by oxidative stress and nutrient deprivation, both of which compromise cell viability and regenerative potential [30]. In the present study, OMT activated the Nrf2/HO-1 signaling axis, thereby strengthening the antioxidant defense capacity of injured cells and preserving mitochondrial redox homeostasis. Consistent with these findings, live/dead staining and hypoxia-associated survival assays further supported the conclusion that OMT improves PMSC survival under hypoxic conditions both in

vitro and in vivo. This cytoprotective effect may be particularly important for transplanted PMSCs, which are highly susceptible to oxidative and ischemic injury after implantation. By mitigating hypoxia-induced damage in both resident wound cells and transplanted PMSCs, OMT may enhance graft persistence and ultimately improve tissue repair outcomes.

This study has several implications. First, it supports the idea that modulating the inflammatory microenvironment is a key therapeutic target for treating refractory wound repair. Second, it indicates that OMT may effectively complement stem cell-based therapy by enhancing cell survival and function in challenging wound environments. Third, combining OMT with PMSCs could be a promising strategy to enhance both structural repair and functional recovery in diabetic wounds.

This study has several limitations that should be acknowledged. Our primary objective was to evaluate the therapeutic efficacy of the OMT+PMSCs combination and to provide preliminary mechanistic insights based on pathway-related expression changes. Therefore, the current mechanistic evidence remains largely associative. Although we observed modulation of TLR4/NF-κB and Nrf2/HO-1 signaling, definitive causal validation (e.g., inhibitor-based intervention, gene silencing/knockdown, or rescue experiments) is still required to establish pathway dependence. In addition, although we provide survival-associated evidence for PMSCs in both in vitro and in vivo contexts, we did not directly characterize changes in paracrine factor secretion after OMT protection, nor did we perform depletion/ablation experiments to determine whether the wound-healing benefit is strictly dependent on transplanted PMSCs survival. Finally, long-term outcomes, including persistence of transplanted PMSCs and durability of regenerated skin appendages, were not fully evaluated. This model still cannot fully recapitulate the chronic complexity of genetically diabetic models (e.g., db/db mice). We will further validate the therapeutic efficacy of OMT+PMSCs in chronic genetic diabetic wound models. Future studies should address these gaps and further examine the translational potential of this strategy in large-animal models and, ultimately, in clinical settings.

In conclusion, OMT combined with PMSC transplantation significantly enhances diabetic wound healing by reducing excessive inflammation, promoting M2 macrophage polarization, boosting antioxidant defenses, aiding cell survival under hypoxic stress, stimulating re-epithelialization, angiogenesis, and skin appendage regeneration. These findings offer a mechanistic basis for a new combinational strategy to treat refractory wounds.

Acknowledgements

This work was financially supported by Ningxia Key Research and Development Program Project 2022BEG03147.

Disclosure of conflict of interest

None.

Address correspondence to: Shudan Liu and Dongmei Chen, Key Laboratory of Ningxia Stem Cell and Regenerative Medicine, Institute of Medical Sciences, General Hospital of Ningxia Medical University, No. 804, Shengli Street, Xingqing District, Yinchuan 750004, Ningxia Hui Autonomous Region, China. Tel: +86-13619589699; E-mail: sky_198566@163.com (SDL); Tel: +86-183096-79151; E-mail: Chendm1981@163.com (DMC)

References

[1] Genitsaridi I, Salpea P, Salim A, Sajjadi SF, Tomic D, James S, Thirunavukkarasu S, Issaka A, Chen L, Basit A, Luk AOY, Ma RCW, Mbanya JC, Ramachandran A, Wild SH, Duncan BB, Boyko EJ and Magliano DJ. 11th edition of the IDF diabetes atlas: global, regional, and national diabetes prevalence estimates for 2024 and projections for 2050. Lancet Diabetes Endocrinol 2026; 14: 149-156.

[2] Hanlon M, McGuire BE, MacGilchrist C, Kirwan E, Neachtain DN, Dhatariya K, Blanchette V, Durand H, Dragomir A and McIntosh C. Beyond the wound: a scoping review of the psychosocial impact of diabetes-related foot ulcers. Diabet Med 2026; 43: e70243.

[3] Wu J, Yang Q, Cheng H, Zheng H and Chen M. Metabolism, senescence, and natural products: new perspectives on wound healing in diabetes. Front Nutr 2026; 12: 1746827.

[4] Ormazabal V, Nova-Lampeti E, Rojas D, Zuniga FA, Escudero C, Lagos P, Moreno A, Pavez Y, Reyes C, Yanez M, Vidal M, Cabrera-Vives G, Oporto K and Aguayo C. Secretome from human mesenchymal stem cells-derived endothelial cells promotes wound healing in a type-2 diabetes mouse model. Int J Mol Sci 2022; 23: 941.

[5] Ahmadieh-Yazdi A, Karimi M, Afkhami E, Hajizadeh-Tafti F, Kuchakzadeh F, Yang P and Sheykhhasan M. Unveiling therapeutic potential: adipose tissue-derived mesenchymal stem cells and their exosomes in the management of diabetes mellitus, wound healing, and chronic ulcers. Biochem Pharmacol 2024; 226: 116399.
[6] Li J, Chen S, Wang H, Wang W and Liu Y. Mesenchymal stem cells derived EXO-miR3671 delivery promoted angiogenesis and accelerated wound healing of diabetes. Stem Cells 2026; 44: sxag008.
[7] Lu D, Yu W, Zhao D, Qi F, Wang X, Fu Q, Li J, Yang F, Li R, Wang X, Lan H, Wang J, Zhang H, Liu D, Wang J and Zhao X. Copper ion-chelated supramolecular polymer/hyaluronic acid hydrogel promotes wound healing in diabetes. Int J Biol Macromol 2025; 319: 145615.
[8] Sun X, Shu J, He J, Cai J, Xu X, Yan F, Luo F, Huang D, Wu Y and Weng Z. Leak-free encapsulation of EGF-expressing yeast in a hyaluronic acid-based hydrogel for diabetes wound healing. Int J Biol Macromol 2026; 337: 149516.
[9] Liu MM, Bai J, Tian ZY, Zheng TT, Boekhout T and Wang QM. Oxymatrine ameliorates malassezia overgrowth-induced psoriasis in vivo and in vitro by inhibiting the biofilm formation and inflammation. Mycology 2025; 17: 2511903.
[10] Ming Z, Liu Y, Jia S, Su Y, Yan W and Lin J. Oxymatrine alleviates symptoms in high-fat diet and STZ-induced SD rats with painful diabetic neuropathy by reducing inflammation and oxidative stress. Front Immunol 2026; 17: 1750051.
[11] Zhu Y, Wu P, Wen R, Tang J, Hou S, Yuan S, Li Z, Li M and Zhao W. Oxymatrine alleviates echinococcus multilocularis infection by remodeling the liver immune microenvironment and intestinal flora homeostasis. Front Cell Infect Microbiol 2025; 15: 1658336.
[12] Kottaisamy CPD, Raj DS, Prasanth Kumar V and Sankaran U. Experimental animal models for diabetes and its related complications-a review. Lab Anim Res 2021; 37: 23.
[13] Ji JY, Ren DY and Weng YZ. Efficiency of multifunctional antibacterial hydrogels for chronic wound healing in diabetes: a comprehensive review. Int J Nanomedicine 2022; 17: 3163-3176.
[14] Li D and Wu N. Mechanism and application of exosomes in the wound healing process in diabetes mellitus. Diabetes Res Clin Pract 2022; 187: 109882.
[15] Fischer BC, Musengi Y, König J, Sachse B, Hessel-Pras S, Schäfer B, Kneuer C and Herrmann K. Matrine and Oxymatrine: evaluating the gene mutation potential using in silico tools and the bacterial reverse mutation assay (Ames test). Mutagenesis 2024; 39: 32-42.
[16] He J, Qin W, Jiang S, Lin Y, Lin Y, Yang R, Xu M and Liu Q. Oxymatrine attenuates sepsis-induced inflammation and organ injury via inhibition of HMGB1/RAGE/NF-κB signaling pathway. Drug Dev Res 2024; 85: e22219.
[17] Xiang J, Wang SQ, Zhang GQ, Jiao LJ, Fu LY, Xu YN, Wang YY, Li X, Tao JL, Yang XY, Cha XS, Tao L and Shen XC. Oxymatrine alleviates atherosclerosis by regulating macrophage senescence via the SIRT1-P53 signaling pathway. Phytother Res 2026; 40: 1173-1194.
[18] Zhou K, Liu D, Jin Y, Xia W, Zhang P and Zhou Z. Oxymatrine ameliorates osteoarthritis via the Nrf2/NF-kappaB axis in vitro and in vivo. Chem Biol Interact 2023; 380: 110539.
[19] Zhang J, Zheng Y, Lee J, Hua J, Li S, Panchamukhi A, Yue J, Gou X, Xia Z, Zhu L and Wu X. A pulsatile release platform based on photo-induced imine-crosslinking hydrogel promotes scarless wound healing. Nat Commun 2021; 12: 1670.
[20] Bhardwaj H, Khute S, Sahu R and Jangde RK. Advanced drug delivery system for management of chronic diabetes wound healing. Curr Drug Targets 2023; 24: 1239-1259.
[21] Huang Y, He B, Song C, Long X, He J, Huang Y and Liu L. Oxymatrine ameliorates myocardial injury by inhibiting oxidative stress and apoptosis via the Nrf2/HO-1 and JAK/STAT pathways in type 2 diabetic rats. BMC Complement Med Ther 2023; 23: 2.
[22] Takeuchi T, Ito M, Yamaguchi S, Watanabe S, Honda M, Imahashi T, Yamada T and Kokubo T. Hydrocolloid dressing improves wound healing by increasing M2 macrophage polarization in mice with diabetes. Nagoya J Med Sci 2020; 82: 487-498.
[23] Wang XL, Chen F, Shi H, Zhang M, Yan L, Pei XY and Peng XD. Oxymatrine inhibits neuroinflammation by Regulating M1/M2 polarization in N9 microglia through the TLR4/NF-κB pathway. Int Immunopharmacol 2021; 100: 108139.
[24] Jiang W, Yao Y and Chen C. Oxymatrine reduces neuropathic pain in diabetic mice through the p38 MAPK/NF-kappaB signaling pathway. Pak J Pharm Sci 2025; 38: 89-100.
[25] Liu M, Liu F, Pan Y, Xiong Y, Zeng X, Zheng L, Zhao H, Li Y and Liu D. Oxymatrine ameliorated experimental colitis via mechanisms involving inflammatory DCs, gut microbiota and TLR/NF-κB pathway. Int Immunopharmacol 2023; 115: 109612.
[26] Ni C, Zhou L, Yang S, Ran M, Luo J, Cheng K, Huang F, Tang X, Xie X, Qin D, Mei Q, Wang L, Xiao J and Wu J. Oxymatrine, a novel TLR2 agonist, promotes megakaryopoiesis and throm-

bopoiesis through the STING/NF-κB pathway. J Pharm Anal 2025; 15: 101054.
[27] Zhang X, Shi J, Lu Y, Ji R, Guan Z, Peng F, Zhao C, Gao W and Gao F. Mechanism of oxymatrine in the treatment of cryptosporidiosis through TNF/NF-κB signaling pathway based on network pharmacology and experimental validation. Sci Rep 2024; 14: 14469.
[28] Baker CJ, Chuter V, Brousseau-Foley M, Min D, Searle A, Twigg SM and Johnson NA. Exercise training for people with diabetes-related foot ulcers: a systematic review of glycemia, fitness, and wound-healing outcomes. Can J Diabetes 2025; 49: 164-173, e1.
[29] Kaussikaa S, Prasad MK and Ramkumar KM. Nrf2 activation in keratinocytes: a central role in diabetes-associated wound healing. Exp Dermatol 2024; 33: e15189.
[30] Xia W, Liu Y, Jiang X, Li M, Zheng S, Zhang Z, Huang X, Luo S, Khoong Y, Hou M and Zan T. Lean adipose tissue macrophage derived exosome confers immunoregulation to improve wound healing in diabetes. J Nanobiotechnology 2023; 21: 128.